Available online at www.sciencedirect.com
ScienceDirect
Journal of Solid State Chemistry 180 (2007) 180–185
JOURNAL OF SOLID STATE CHEMISTRY
www.elsevier.com/locate/jssc

Formation of γ-Fe_2O_3 nanoparticles and vacancy ordering: An *in situ* X-ray powder diffraction study

Jens-Erik Jørgensen[a,*], Lene Mosegaard[a], Line E. Thomsen[a], Torben R. Jensen[a], Jonathan C. Hanson[b]

[a]*Chemistry Department, University of Aarhus, DK-8000 Århus C, Denmark*
[b]*Chemistry Department, Brookhaven National Laboratory, Upton, NY 11973, USA*

Received 9 June 2006; received in revised form 19 September 2006; accepted 27 September 2006
Available online 10 October 2006

Abstract

The formation of maghemite, γ-Fe_2O_3 nanoparticles has been studied by *in situ* X-ray powder diffraction. The maghemite was formed by thermal decomposition of an amorphous precursor compound made by reacting lauric acid, $CH_3(CH_2)_{10}COOH$ with $Fe(NO_3)_3 \cdot 9H_2O$. It has been shown that cubic γ-Fe_2O_3 was formed directly from the amorphous precursor and that vacancy ordering starts about 45 min later at 305 °C resulting in a tripled unit cell along the *c*-axis. The kinetics of grain growth was found to obey a power law with growth exponents *n* equal to 0.136(6) and 0.103(5) at 305 and 340 °C, respectively. Particles with average sizes of 12 and 13 nm were obtained in 86 and 76 min at 305 and 340 °C, respectively. The structure of cubic and vacancy ordered phases of γ-Fe_2O_3 was studied at 305 °C by Rietveld refinements.

Keywords: *In situ* X-ray powder diffraction

1. Introduction

Maghemite (γ-Fe_2O_3) is extensively used for information storage in magnetic discs and tapes. The ever increasing request for higher information storage densities creates a demand for the development of storage media containing ultra-fine magnetic particles [1,2]. The preparation of γ-Fe_2O_3 nanoparticles has therefore evoked a lot of interest and various synthetic methods have been applied for the preparation of γ-Fe_2O_3 particles of which many have been based on the use of aqueous solutions [3–5]. However, products prepared from aqueous solution are often contaminated by ions such as Na^+ and Cl^- [5]. Therefore non-aqueous synthesis methods have been developed. Heyeon et al. [6] have prepared highly crystalline and monodisperse nanoparticles with particle size of 13 nm by direct oxidation of iron pentacarbonyl in the presence of oleic acid using trimethylamine oxide as the oxidating agent. Recently attention has been focussed on the synthesis of γ-Fe_2O_3 nanoparticles from organic precursors [2,7]. These methods offer the advantage of treatment at relatively low temperatures in comparison with conventional methods. The thermal treatment is of importance as γ-Fe_2O_3, which is the ferromagnetic cubic form of iron(III) oxide, on heating transforms to the more stable α-Fe_2O_3 polymorph, which is rhombohedral and antiferromagnetic [8]. The kinetics of the formation of γ-Fe_2O_3 nanoparticles has been studied by Deb and Basumallick [7]. Stearic acid was used as the non-aqueous medium in this study and it was found, that γ-Fe_2O_3 was formed by a nucleation and growth type process having an activation process of 115 kJ/mol. Furthermore, acicular shaped γ-Fe_2O_3 nanoparticles with major and minor axis of 17 and 1.7 nm, respectively, have been prepared by using lauric acid as the non-aqueous medium by Jing and Wu [9]. This study indicated that particle size, thermal stability and magnetic properties of the prepared particles strongly depend on the conditions of preparation.

*Corresponding author. Fax: +45 8942 6199.
E-mail address: jenserik@chem.au.dk (J.-E. Jørgensen).

0022-4596/$ - see front matter © 2006 Elsevier Inc. All rights reserved.
doi:10.1016/j.jssc.2006.09.033

The structure of γ-Fe_2O_3 is closely related to the structure of magnetite (Fe_3O_4) which possesses the inverse spinel structure but it differs from magnetite by the presence of iron vacancies [10]. The formula of γ-Fe_2O_3 can be written as $Fe_{21\ 1/3}\square_{2\ 2/3}O_{32}$ as 11.1% of the iron sites are vacant ($\square$ represents a vacant iron site). Vacancy ordering gives rise to different crystal symmetries and three possible models for the distribution of vacancies have been suggested: (1) cubic structure with random distribution of the vacancies (space group *Fd*-3*m*); (2) vacancies distributed as the Li cations in $LiFe_5O_8 = Fe_8[Li_4Fe_{12}]O_{32}$ (space group $P4_332$); and (3) an ordered distribution of the vacancies with tetragonal symmetry and a three-fold doubling along the *c*-axis (space group $P4_12_12$) [10,11]. It has been shown that the cation vacancy distribution depend on the preparation method of γ-Fe_2O_3.

In this study, we present an *in situ* X-ray powder diffraction study of the formation and thermal stability of γ-Fe_2O_3 nanoparticles prepared by using lauric acid as the non-aqueous medium and $Fe(NO_3)_3 \cdot 9H_2O$ as the iron source.

2. Experimental

The samples studied by *in situ* X-ray diffraction were prepared as follows: $Fe(NO_3)_3 \cdot 9H_2O$ was added to molten lauric acid, $CH_3(CH_2)_{10}COOH$ in the molar ratio of 1:1. The homogeneous mixture was heated in a beaker at 120 °C under vigorous stirring and evolution of brown NO_2 gas was observed. A sticky moist red-brown mass was formed and it was cooled down to room temperature in air. Thereafter, it was treated with 100 mL of tetrahydrofuran yielding a brown precipitate which was dried at 70 °C in air for 4 h to form the precursor powder of the amorphous FeOOH.

The *in situ* X-ray powder diffraction work was performed on the X7B beam line at NSLS, Brookhaven National Laboratory, USA. The precursor powder was loaded into quartz capillary tubes with diameters in the size range 0.5–0.7 mm. The quartz capillary tube was placed inside a sapphire tube with open access to the air and it was heated by a resistive heating element. The temperature was measured with a chromel–alumel thermocouple placed inside the sapphire tube and next to the sample. Powder patterns were recorded in the temperature range from 280 to 365 °C using the image plate area detector (Model MAR345) and X-rays of wavelength $\lambda = 0.92191$ Å. Each image was exposed for 60 s and the total time resolution of the experiment was 146 s (exposure time plus read-out time for the image plate) per powder pattern. The recorded images were subsequently converted to powder patterns using the FIT2D software package [12]. The crystal structure of the prepared γ-Fe_2O_3 nanoparticles was studied by the Rietveld method using the GSAS suite of programs [13].

3. Results and discussion

3.1. Formation of γ-Fe_2O_3

The growth process of γ-Fe_2O_3 was studied at the following temperatures: 280, 305 and 340 °C. Samples were heated with heating rates of 21.4 °C/min to the final temperature for the measurement and kept at this temperature for up to 90 min. An additional sample was heated to 365 °C with a heating rate of 42.5 °C/min. It was found that the γ-Fe_2O_3 phase did not form at 280 °C within 60 min while the formation of this phase at 365 °C was too fast to be studied by the time resolution of the present experiment. Fig. 1 shows a stack of powder diagrams recorded for the sample heated to 305 °C. The precursor material is seen to be amorphous or poorly crystalline. The formation of γ-Fe_2O_3 (marked with an arrow) starts at $t = 16$ min which is about 4 min after the temperature had reached 305 °C. No intermediate crystalline phases are observed. Super-lattice reflections are seen to appear about 41 min later ($t = 57$ min). The reflections of powder patterns recorded between $t = 16$ and 57 min were indexed on a F-centred cubic unit cell with $a \approx 8.40$ Å, while the reflections of patterns recorded at times later than 57 min were indexed on a primitive tetragonal unit cell with $a \approx 8.34$ Å and $c \approx 3a$. The appearance of super-lattice reflections is due to the ordering of iron cation vacancies as described in more detail below. The sample ramped to 340 °C showed qualitatively the same behaviour as the one ramped to 305 °C. The formation of the γ-Fe_2O_3 started about 1 min after the temperature of 340 °C was reached and the vacancy ordering started 32 min later.

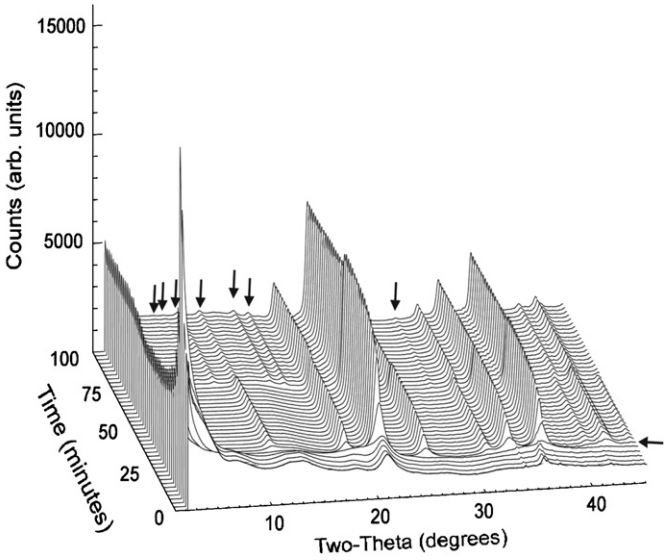

Fig. 1. Stack of powder diagrams recorded at 305 °C. The temperature of 305 °C was reached in 13 min and the formation of the γ-Fe_2O_3 phase starts about 4 min later. The onset of vacancy ordering is clearly seen after an additional 45 min at 305 °C. The arrows mark selected super lattice peaks as described in the text.

In addition to the above described measurements a stack of powder diagrams were recorded during the temperature ramp from 25 to 400 °C with the heating rate of 3.1 °C/min. No formation of the γ-Fe_2O_3 phase was observed in this measurement but formation of haematite, α-Fe_2O_3 started at 338 °C and no intermediate crystalline phases are observed.

The crystallisation of both the α-Fe_2O_3 and γ-Fe_2O_3 phases was found to be accompanied by an increase in the scattering at low angles going through a maximum just before the onset of crystallisation. However, the setup used in this experiment does not allow a detailed study of the time dependence of the small angle scattering. This phenomena was also observed in an *in situ* X-ray diffraction study of the crystallisation of microporous aluminophosphates by Christensen et al. [14].

3.2. Particle size

The average particle sizes D were determined from the full-width of half-maximum of the (311) reflection of the cubic phase using the Scherrer equation:

$$B(2\theta) = 0.94\lambda/D \cos\theta, \quad (1)$$

where $B(2\theta)$ is the full-width of half-maximum due to particle broadening and 2θ and λ are the scattering angle and wave length, respectively. The full-width of half-maximum $B(2\theta)$ was corrected for instrumental intrinsic line broadening assuming gaussian line shape and $B(2\theta\text{intrinsic}) = 0.15°$. The particle size was also estimated from the full-width of half-maximum of the (110) reflection and no significant difference between particle sizes determined from the (311) and (110) reflections was found. Furthermore, no evidence of non-spherical particles was found in the Rietveld refinements described below and the particles were therefore assumed to be spherical. Fig. 2 shows particle size as a function of time at 305 and 340 °C while the inset of this figure shows the integrated intensity of the (311) reflection as a function of time. The average particle size increases from 7.5 to 11.5 nm in 44 min at 305 °C within the cubic phase. An average particle size of 12.5 nm was reached in 30 min at 340 °C also within the cubic phase. The integrated intensity of the (311) reflection raises sharply to its maximum value within on powder pattern (less than ca. 2.5 min). The fact that the growth rate of the integrated intensity is much faster than the growth rate of the average particle size indicates that the whole sample transforms from the amorphous state to a nano-crystalline γ-Fe_2O_3 phase within the above mentioned time frame. Thereafter the average particle size increases, presumably as larger particles grow at the expense of smaller ones. The time resolution of the experiment does not allow a study of the very early stages of the growth process of the cubic γ-Fe_2O_3 particles. Within the investigated time range it was found that the average particle size D is well described by a power law as described below.

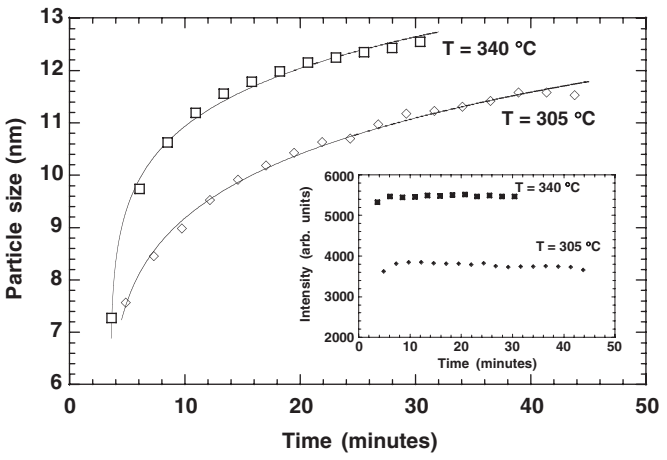

Fig. 2. Average particle sizes plotted as function of time at 305 and 340 °C. The solid lines represent fits to power laws as described in the text. The inset shows the intensity of the (311) reflection as a function of time.

3.3. Kinetics of the growth of the nano-particles

The kinetics of grain growth in polycrystalline materials has been studied by theoretical and experimental methods as well as by computer simulations and the topic has been reviewed by Atkinson [15]. Under ideal conditions grain growth takes place to decrease the system energy by decreasing the total grain boundary energy. The growth rate is proportional to the curvature of the grain boundary and thereby to the inverse grain diameter $1/D$. Grain growth kinetic are under these conditions described by the relation:

$$D(t) = k(t - t_0)^n \quad (2)$$

with $n = 1/2$, assuming zero grain diameter at $t = t_0$, Burke and Turnbull [16]. Experimental determinations of grain growth exponents have shown that $n = 1/2$ is obtained in pure metallic systems only, while $n < 1/2$ is obtained in most other cases. In the present work grain growth exponents n equal to 0.136(6) and 0.103(5) were obtained at 305 and 340 °C, respectively. The obtained grain growth exponent is considerably smaller than 1/2 and similar values have only been found in a few other studies: In the case of mullite a value of $n \approx 1/12$ was found for annealing temperatures below 1600 °C [17] and a study of grain growth in nanocrystalline iron yielded growth exponents in the range 0.1–0.5 and increasing with temperature [18]. The changes in particle size in the vacancy ordered phases are minor at 305 and 340 °C and the grain sizes determined from the last scans recorded at these temperatures are 12 and 13 nm, respectively.

3.4. Structural investigation of vacancy disordered γ-Fe_2O_3

The crystal structure of γ-Fe_2O_3 was studied by Rietveld refinements performed on data recorded at 305 °C. Data

sets recorded after 22 and 63 min at 305 °C, which corresponds to the cubic and vacancy ordered phase, respectively, were used in the refinements. Several trial refinement of the structure of cubic γ-Fe_2O_3 were performed in space group *Fd*-3*m* as well as in space group $P4_332$ although the indexing procedure indicated an F-centred unit cell. The simplest description of the cubic form of γ-Fe_2O_3 is done in space group *Fd*-3*m* in which only one structural parameter is present while a description in space group $P4_332$ requires six structural parameters. The best refinement was obtained in space group *Fd*-3*m* and the results of this refinement for data recorded at 305 °C are given in Table 1 and the observed and calculated powder patterns are shown in Fig. 3. During the refinement it was assumed that the oxygen lattice was fully occupied and the occupancies of the 8*a* and 16*d* iron sites were constrained to obey the 2:3 stochiometry during the refinements. Isotropic thermal displacement parameters were used for iron and oxygen and only one common parameter was used for the two crystallographically independent iron atoms. The octahedral 16*d* and tetrahedral 8*a* sites were found to contain 9.8(1)% and 13.8(1)% vacancies, respectively. This is in contrast to the majority of earlier studies, which show that the iron vacancies mainly occupy octahedral position [19–21]. However, Kryukova et al. [22] have proposed a model with ordered iron vacancies on both octahedral and tetrahedral sites. This model was based upon simulation of high-resolution electron micrographs of γ-Fe_2O_3. The distribution of iron vacancies over both tetrahedral and octahedral sites might be due to the fact that the present data set was recorded at elevated temperature which favours a model with higher entropy. The fact that the present refinement is based on data recorded shortly after the formation of the γ-Fe_2O_3 phase and at elevated temperature and makes a direct comparison with other room temperature structural studies of γ-Fe_2O_3 difficult. The Fe–O bond lengths for tetrahedrally and octahedrally bonded iron were found to be 1.837(3) and 2.091(2) Å, respectively, in the cubic vacancy disordered phase.

Table 1
Structural parameters for cubic γ-Fe_2O_3 refined using powder diffraction data measured after 22 min at $T = 305$ °C

Atom	Position	x	y	z	occ.
Fe	8*a*	$\frac{1}{8}$	$\frac{1}{8}$	$\frac{1}{8}$	0.865(1)
Fe	16*d*	$\frac{1}{2}$	$\frac{1}{2}$	$\frac{1}{2}$	0.901(1)
O	32*e*	0.2512(2)	0.2512(2)	0.2512(2)	1.0

Space group *Fd*-3*m* (#227), $a = 8.4053(1)$ Å. Thermal displacement parameters: $\langle u^2_{Fe}\rangle = 0.0144(3)$ Å^2 and $\langle u^2_{O}\rangle = 0.0251(6)$ Å^2. $R_p = 0.0136$, $R_{wp} = 0.0200$, $R_{exp} = 0.0280$, $R(F^2) = 0.0166$, $\chi^2 = 0.511$, number of reflections = 21 and number of parameters = 22.

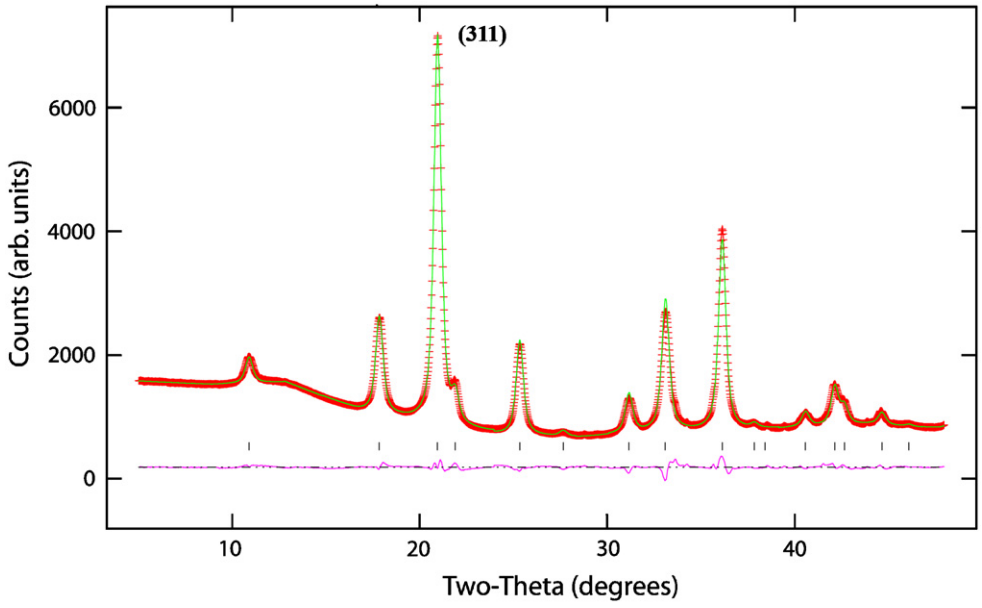

Fig. 3. X-ray powder diffraction pattern of cubic the γ-Fe_2O_3 recorded at 305 °C. The Rietveld refinement was done in space group *F*d-3m. The crosses and the solid line represent the measured and calculated patterns, respectively. The lower curve shows the difference between observed and calculated intensities and the vertical tick marks show the position of the Bragg reflections. The (311) reflection used for particle size determination is marked on the figure.

3.5. Structural investigation of vacancy ordered γ-Fe_2O_3

The appearance of weak super-lattice peaks after about 45 min at 305 °C indicates ordering of the vacancies and thereby a lowering of the symmetry from cubic to tetragonal. Indexing was done on a primitive unit cell with $a' = b' \approx a$ and $c' \approx 3a$, where a', b' and c' are the lattice parameters for the tetragonal structure while a is the lattice parameter for the cubic structure. The observation of very weak super-lattice reflections at $2\theta = 6.68°$ and 7.61° with Miller indices (1 0 1) and (1 0 2), respectively, confirms the tripling of the unit cell. The space group of the tetragonal vacancy-ordered phase is $P4_12_12$ [23]. A powder pattern recorded about 18 min after vacancy ordering was used for the Rietveld refinement of the vacancy-ordered phase. The tripled unit cell contains 59 positional parameters which in combination with the limited observed number of reflections prevents an unconstrained refinement of the structure. Therefore an average tetragonal unit cell with $a' = b' \approx a$, $c' \approx a$ and space group $P4_32_12$ was used for initial trial refinements. This type of model was also used in a neutron powder diffraction study of γ-Fe_2O_3 by Greaves [24]. $P4_12_12$ is a maximal isomorphic subgroup of $P4_32_12$ and just 20 positional parameters are required in the $P4_32_12$ model. The four crystallographically independent Fe and O atoms are located in 4*a* (x x 0) and 8*b* (x y z) positions in space group $P4_32_12$. The site occupancy of one of the iron atom located in a 4*a* position was fixed at 1/3 during the initial refinements to preserve the chemical 2:3 stoichiometry while the remaining sites were fully occupied. The structural parameters obtained in the trial refinements in space group $P4_32_12$ was then transformed to space group $P4_12_12$. The transition from space group $P4_32_12$ to $P4_12_12$ causes a 4*a* position to split into a 4*a* and an 8*b* position while an 8*b* position is split into three 8*b* positions. The results of the Rietveld refinement in space group $P4_12_12$ is given in Table 2 and the observed and calculated powder patterns are shown in Fig. 4. All atoms except Fe9 were

Table 2
Structural parameters for vacancy ordered tetragonal γ-Fe_2O_3 refined using powder diffraction data measured after 63 min at $T = 305$ °C

Atom	Position	x	y	z
Fe1	8*b*	0.751(2)	0.997(2)	0.0417(5)
Fe2	8*b*	x_{Fe1}	y_{Fe1}	$z_{Fe1}+1/3$
Fe3	8*b*	x_{Fe1}	y_{Fe1}	$z_{Fe1}+2/3$
Fe4	4*a*	0.621(3)	0.621(3)	0.0
Fe5	8*b*	x_{Fe4}	y_{Fe4}	
Fe6	8*b*	0.369(2)	0.869(2)	0.998(1)
Fe7	8*b*	x_{Fe6}	y_{Fe6}	$z_{Fe6}+1/3$
Fe8	8*b*	x_{Fe6}	y_{Fe6}	$z_{Fe6}+2/3$
Fe9	4*a*	0.128(3)	0.128(3)	0.0
O1	8*b*	0.612(7)	0.881(6)	0.000(2)
O2	8*b*	x_{O1}	y_{O1}	$z_{O1}+1/3$
O3	8*b*	x_{O1}	y_{O1}	$z_{O1}+2/3$
O4	8*b*	0.110(4)	0.317(3)	0.003(1)
O5	8*b*	x_{O4}	y_{O4}	$z_{O4}+1/3$
O6	8*b*	x_{O4}	y_{O4}	$z_{O4}+2/3$
O7	8*b*	0.133(7)	0.853(3)	0.000(2)
O8	8*b*	x_{O7}	y_{O7}	$z_{O7}+1/3$
O9	8*b*	x_{O7}	y_{O7}	$z_{O7}+2/3$
O10	8*b*	0.385(6)	0.626(3)	0.006(2)
O11	8*b*	x_{O10}	y_{O10}	$z_{O10}+1/3$
O12	8*b*	x_{O10}	y_{O10}	$z_{O10}+2/3$

$a = 8.332(1)$ Å, $c = 25.113(6)$ Å. Thermal displacement parameters: $\langle u^2_{Fe}\rangle = 0.0144(3)$ Å^2 and $\langle u^2_O\rangle = 0.0251(6)$ Å^2. $R_p = 0.0201$, $R_{wp} = 0.0275$, $R_{exp} = 0.0289$, $R(F^2) = 0.0637$, $\chi^2 = 0.903$, number of reflections = 480 and number of parameters = 29.

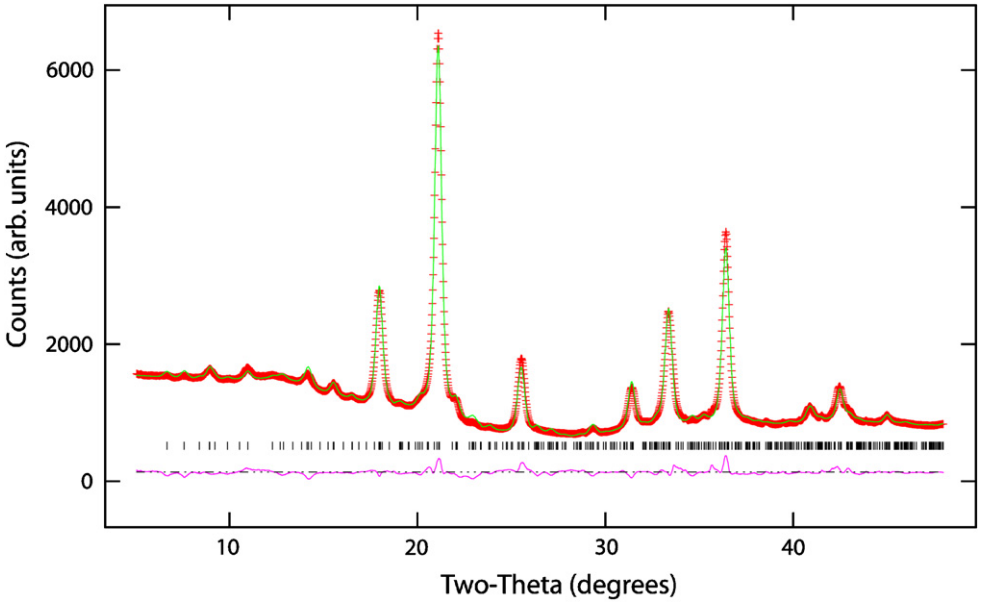

Fig. 4. X-ray powder diffraction pattern of tetragonal vacancy ordered γ-Fe_2O_3 recorded after 63 minutes at 305 °C. The Rietveld refinement was done in space group $P4_12_12$ and the crosses and solid line represent the measured and calculated patterns, respectively. The lower curve shows the difference between observed and calculated intensities and the vertical tick marks show the position of the Bragg reflections.

constrained to follow $P4_32_12$ symmetry as seen from Table 2. The partially occupied 4*a* iron position in space group $P4_32_12$ transforms into a fully occupied 4*a* position (Fe9) in space group $P4_12_12$ while the corresponding 8*b* position is unoccupied thereby preserving the chemical 2:3 stoichiometry. The iron vacancies are in this way fully ordered and confined to octahedral sites. The Fe–O bond lengths for tetrahedrally coordinated Fe were found to be within the range of 1.76(5)–2.17(2) Å. The corresponding bond length range for octahedrally coordinated Fe was found to be 1.64(3)–2.24(4) Å. As seen from Fig. 4, the intensities of the super-lattice reflections are well accounted for by the $P4_12_12$ model thereby showing that the iron vacancies are fully ordered on the tripled unit cell. Furthermore, the shape of the super-lattice reflections are well described by the profile function used in the Rietveld refinements and it is therefore concluded that the sample consists of single domain vacancy ordered nanoparticles.

4. Conclusion

It has been shown by *in situ* X-ray powder diffraction that γ-Fe_2O_3 forms directly from an amorphous precursor material made from lauric acid and $Fe(NO_3)_3 \cdot 9H_2O$. The amorphous precursor transforms to nano-crystalline γ-Fe_2O_3 in less than 2.5 min, which was the time resolution of the experiment. The average particle size was found to increase as a function of time as larger particles grow at the expense of smaller ones. The kinetics of grain growth was found to obey a power law with growth exponents n equal to 0.136(6) and 0.103(5) at 305 and 340 °C, respectively. Average particle sizes of 12 and 13 nm were obtained in 86 and 76 min at 305 and 340 °C, respectively. Initially γ-Fe_2O_3 is formed in its cubic form with disordered cation vacancies. The cubic γ-Fe_2O_3 phase was found to transform to the vacancy ordered phase resulting in a triplication along the *c*-axis. The life time of the cubic phase was found to be 41–32 min in the temperature range 305–340 °C and the vacancies were found to order almost completely with in time resolution of 146 s of the experiment. Furthermore, Rietveld refinements showed that the structure of the cubic phase is best described in space group *Fd*-3*m* while the structure of the vacancy ordered phase was refined as a constrained refinement in space group $P4_12_12$ showing that the iron vacancies are fully ordered on the tripled unit cell.

Acknowledgment

The authors would like to thank Dansync for financial support. The synchrotron X-ray measurements were carried out at Brookhaven National Laboratory, supported under contract. TRJ is grateful to Carlsberg Fondet for financial support.

References

[1] T. Ishikawa, T. Takeda, R.K. Kandori, J. Mater. Sci. 27 (1992) 4531–4535.
[2] G. Ennas, G. Marogui, A. Misinu, A. Falqui, P. Ballirano, R. Caminiti, J. Mater. Res. 14 (1999) 1570–1575.
[3] B.R.V. Narasimban, S. Prabhakar, Mater. Lett. 52 (2002) 52, 295–300.
[4] M.P. Morales, M.A. Verges, J. Magn. Magn. Mater. 203 (1999) 146–148.
[5] Y. Konshi, T. Kawamura, S. Asai, Ind. Eng. Chem. Res. 32 (1993) 2888–2891.
[6] T. Heyeon, S.S. Lee, J. Park, J. Am. Chem. Soc. 123 (2001) 12798–12801.
[7] P. Deb, A. Basumallick, J. Nanoparticle Res. 6 (2004) 527–531.
[8] M.P. Morales, C. Pecharroman, C.T. Gonzales, C.J. Cerna, J. Solid State Chem. 108 (1994) 158–163.
[9] Z. Jing, S. Wu, J. Solid State Chem. 177 (2004) 1213–1218.
[10] G.W. Oosterhout, C.J.M. Rooymans, Nature (London) 181 (1958) 44–46.
[11] P.B. Braun, Nature (London) 179 (1952) 1123.
[12] A.P. Hammersley, ESRF Internal Report, ESRF97HA02T, "FIT2D: An introduction and Overview", 1997.
[13] A.C. Larson, R.B. Von Dreele, Los Alamos National Laboratory Report no. LA-UR-86-748, 1987.
[14] A.N. Christensen, T.R. Jensen, P. Norby, J.C. Hanson, Chem. Mater. 10 (1998) 1688–1693.
[15] H.V. Atkinson, Acta Metall. 36 (1988) 469–491.
[16] J.E. Burke, D. Turnbull, Prog. Met. Phys. 3 (1952) 220–292.
[17] M. Schmücker, H. Schneider, T. Mauer, B. Clauss, J. Am. Ceram. Soc. 88 (2005) 488–490.
[18] T.R. Marlow, C.C. Koch, Acta Mater. 45 (1997) 2177–2186.
[19] R. Uyeda, K. Hasegava, J. Phys. Soc. Jpn. 17 (Suppl. B-II) (1962) 391–394.
[20] K. Haneda, A.H. Morrish, Solid State Commun. 22 (1977) 779–781.
[21] R.J. Armstrong, A.H. Morrish, G.A. Savatsky, Phys. Lett. 23 (1966) 414–416.
[22] G.N. Kryukova, A.L. Chuvilin, V.A. Sadykov, J. Solid State Chem. 89 (1990) 208–211.
[23] A.N. Shmakov, G.N. Kryukova, S.V. Tsybulya, A.L. Chuvilin, L.P. Solovyeva, J. Appl. Crystallogr. 28 (1995) 141–145.
[24] C. Greaves, J. Solid State Chem. 49 (1983) 325–333.